

Effect of UV exposure on the microstructure and mechanical properties of long fiber thermoplastic (LFT) composites

A. Goel · K. K. Chawla · U. K. Vaidya ·
M. Koopman · D. R. Dean

Received: 24 October 2007 / Accepted: 28 December 2007 / Published online: 18 April 2008
© Springer Science+Business Media, LLC 2008

Abstract In this work, the effect of ultraviolet (UV) exposure on the microstructure and dynamic Young's modulus of polypropylene (PP)/21 vol.% E-glass LFT and neat PP was investigated. Microscopic observations revealed that the damage due to UV was confined to the surface region only in the form of surface cracking and exposure of fibers to the surface in the case of long fiber thermoplastic (LFT) and surface cracking in the case of neat PP. Fourier transform infrared spectroscopy showed that the crystallinity of PP in the damaged layer increased, both in neat PP as well as in LFT, with exposure time. This is due to chemicrystallization, which involves rearrangement of amorphous broken polymer chains into crystalline form. Crystallinity of PP in the damaged layer in LFT increased at a higher rate as compared to that in neat PP. Results of nanoindentation showed that the Young's modulus of the PP in the damaged layer increased, with UV exposure time; the rate of modulus increase being higher in the case of LFT than in neat PP. Although the local

Young's modulus of the degraded layer increased, the dynamic Young's modulus of the overall composite showed a decrease with UV exposure time.

Introduction

Thermoplastic matrix composites are increasingly used in a variety of applications such as mass-transit, automotive, and military structures. They hold a distinctive edge over traditional materials, such as steel and aluminum, in these applications due to their high specific strength, good damping capacity, and corrosion resistance [1]. The matrix in thermoplastic composites is generally comprised of polypropylene (PP), polyethylene (PE), nylon, or other inexpensive polymers. E-glass fiber is a commonly used reinforcing material. Long fiber thermoplastic (LFT) composites have seen fairly high growth rates in the plastics industry. The fibers in LFTs have large fiber aspect ratio [ratio of length (ℓ) to diameter (d)], often $\ell/d > 1,000$ and thus take full advantage of the reinforcing fiber strength [2]. The final fiber lengths in the composite are typically >13 mm.

Long fiber thermoplastics are frequently used for outdoor structural applications and are exposed to UV radiation. Hence, it is important to investigate the effect of UV exposure on mechanical properties of these materials. LFTs provide enhanced stiffness to the structural part due to the reinforcing fiber. An obvious disadvantage of using these composites in outdoor applications, however, is their susceptibility to environmental degradation especially due to solar radiation. The wavelength of solar radiation ranges from 290 to 1,400 nm. The infrared region (780–1,400 nm) comprises $\sim 53\%$ of

A. Goel · K. K. Chawla (✉) · U. K. Vaidya · M. Koopman ·
D. R. Dean
Department of Materials Science and Engineering,
University of Alabama at Birmingham, BEC 254,
1530 3rd Ave. S, Birmingham, AL 35294-4461, USA
e-mail: kchawla@uab.edu

A. Goel
e-mail: ashutosh@uab.edu

U. K. Vaidya
e-mail: uvaidya@uab.edu

M. Koopman
e-mail: mkoopman@uab.edu

D. R. Dean
e-mail: deand@uab.edu

the spectrum, while the visible region (400–780 nm) comprises of about 43% and the ultraviolet (UV) region (290–400 nm) constitutes of 4% of the total radiation. The energy of a photon is inversely proportional to its wavelength; hence, the low-wavelength UV region has more energy and thus can be more damaging to the chemical structure of the polymer matrices as compared to the visible light [3]. The photodegradation of polymers depends on external as well as some internal factors. The external factors include wavelength, irradiation time, intensity, temperature, oxygen partial pressure, etc.; while the internal factors include molecular structure of the polymer and its defects, degree of tacticity, fabrication procedure, internal impurities, such as chromophores, and specimen thickness. It has been well documented in the literature that polymers degrade through a photo-oxidative reaction, which is governed by the diffusion of oxygen [4]. Formation of various chemical groups such as carbonyl, hydroperoxide, carboxylic acid, and γ -lactone in the photochemical degradation of PP has been confirmed by previous researchers [5]. Photo-oxidation starts with the absorption of photons by the polymer and subsequent generation of free radicals. The free radicals generated rapidly react with oxygen to form peroxy radicals. This removes hydrogen atoms from the polymer to form alkyl radicals and hydroperoxide. Hydroperoxide decomposes to alkoxy and hydroxyl. These very reactive radicals further remove hydrogen atoms from the polymer to yield new alkyl radicals [3].

Degradation of thermoplastic matrix composites due to UV exposure is a very important topic. Some work on UV degradation of natural fibers reinforced thermoplastics such as PE has been reported [6, 7]. These works reported a comparative study of the degradation of neat PE, PE with additives, and PE with fibers in terms of the changes in flexural modulus and flexural strength with UV and moisture exposure. The flexural modulus of PE reinforced with natural fibers (wood and kenaf) decreased with exposure time. The flexural modulus of pure PE increased during the first 2,000 h of exposure to UV due to cross-linking but decreased later due to chain scission. The flexural modulus of stabilized HDPE also decreased with time although a little bit less than the unstabilized PE.

Work has also been done on the UV degradation of the neat PP [4, 5, 8–11] and some work on the reinforced PP [4, 9]. Most of the past work on UV degradation of neat PP has focussed on studying the mechanism of photodegradation of PP and relating the mechanical property changes with the changes in crystallinity and the surface cracking of the matrix. According to these authors [4, 5, 8–11], chemically crystallization, which is the rearrangement of broken polymer chains into crystalline phase, causes an increase in crystallinity. This is one of

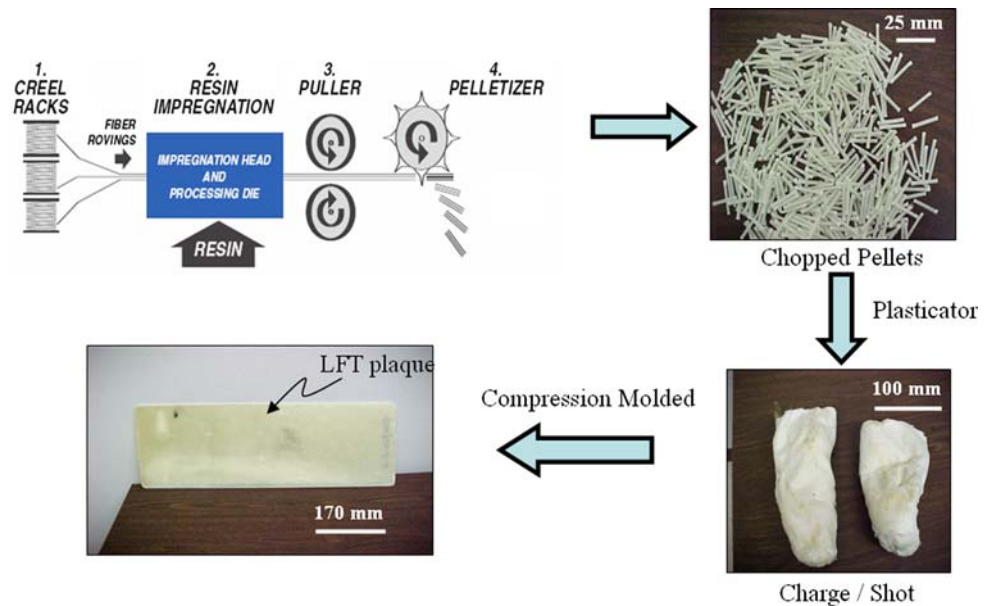
the main results of photodegradation of PP. Chemically crystallization causes surface cracks which is the primary cause for degradation of bulk mechanical properties. Not much work has been done to study the effect of UV exposure on the changes in mechanical properties of the LFT. Also detailed characterization of the mechanical properties of the degraded surface layer, formed due to UV exposure, has not been done. The aim of the current work was to investigate the effect of UV exposure on the mechanical properties of LFT [E-glass (21 vol.%) / PP] produced by the extrusion–compression molding process. In particular, we studied the local changes taking place in the structure such as degree of crystallinity and mechanical properties such as modulus of the degraded layer formed due to UV exposure by Fourier transform infrared (FTIR) spectroscopy and nanoindentation. A comparative study was also done with neat PP in order to evaluate the effect of glass fibers on the local damage caused due to UV exposure.

Experimental

Processing

A schematic of the process for the LFT plaques is shown in Fig. 1. A hot-melt impregnation process was used to produce impregnated glass fiber tows. In this process the fiber tows were pultruded through a heated die during which the individual filaments are wet-out with PP. The pultruded tow impregnated with the PP matrix was cooled and then chopped into LFT pellets of 25-mm length. In the present work such glass fiber/PP LFT pellets (Celstran[®] PP-GF-40-03, Ticona, Florence, KY) were used as a starting material for an extrusion/compression molding process. A plasticator and 400-ton capacity compression molding press were used. The plasticator converts the LFT pellet into a bulk molten charge. The pressure in the plasticator was 1.25 MPa, the screw speed 9–10 rpm, and the melt temperature at the knife was 232 °C. The molten charge was then quickly transferred to a press where it was compression molded while still hot. Plaques fabricated with the 400-ton force were used in the current work. The mold temperature, checked every 40 cycles, remained constant at 54 and 76 °C for the top and bottom halves of the mold, respectively. The plaque temperature at the time of ejection ranged from 87.5 to 90.0 °C and from 45 to 51 °C 5 min after ejection, for an ambient temperature of 31–32 °C. The plaques were then removed after cooling. Rectangular LFT plaques of 21 vol. % long E-glass fiber reinforced and of dimensions $600 \times 240 \times 4 \text{ mm}^3$ were then obtained [1].

Fig. 1 A schematic of the fabrication process of LFT plaques (Courtesy of S.D. Bartus)



UV exposure

Ultraviolet exposure was done in RPR 200 (Rayonet, Branford, CT) reactor with 12 fluorescent bulbs that provided UV radiation at wavelengths of 300–400 nm within the chamber. All the specimens were placed at the center of the reactor. The intensity reading at the center of the reactor was 92 W/m² and the wavelength of about 90% of the UV radiation was ~350 nm. The specimens were removed after 100, 200, 400, 800, 1,200, and 1,600 h of exposure.

Optical microscopy

Microstructure of the cross section of LFT composites after UV degradation was examined by optical microscopy. The cross sections were mounted in epoxy resin and polished using 320, 500, 1,200, 4,000 grit SiC papers followed by 1 μm Al₂O₃ slurry, using a Struers automatic polisher (Struers Inc., Westlake, OH). An optical microscope, ZEISS AXIOPLAN, was used to observe the as-polished cross sections.

Scanning electron microscopy

The surface of the UV degraded sample was examined using a Philips SEM 515 (Philips, Eindhoven, The Netherlands). The samples were first ultrasonically cleaned and then sputter coated with gold/palladium to provide surface conductivity. Unexposed samples, as well as samples exposed to UV, were examined to analyze the damage caused by UV exposure.

Nanoindentation

A commercial nanoindenter (MTS Nano Indenter XP-II, Minneapolis, MN) was used to perform nanoindentation on the polished cross section of the UV degraded neat PP and the PP matrix in the LFT. A continuous stiffness measurement (CSM) technique was used in all experiments [12]. This technique consists of applying a small oscillation to the force signal at a high frequency during indentation loading. The amplitude of the force oscillation is kept small. The contact stiffness is measured by the displacement response at the excitation frequency. The Young’s modulus is then derived from the contact stiffness. The main advantage of this technique is that the modulus can be evaluated as a function of indentation depth. Indentation was conducted with a Berkovich indenter under displacement control at a displacement rate of 10 nm/s. The depth of indentation was kept constant at 2 μm. Indentations were done both on the UV degraded as well as unaffected region and then modulus was calculated by taking the average of ten indentations at a given depth, from the surface.

Contact stiffness, *S*, is obtained by the following relation from the CSM technique [12, 13]:

$$S = \left[\frac{1}{\frac{P_{OS}}{h(\omega)} \cos \varphi - (K_s - m\omega^2)} - K_f^{-1} \right]^{-1}, \tag{1}$$

where *P*_{OS} is the peak value of the harmonic force, *h*(*ω*) is the magnitude of the indenter displacement when the harmonic force is applied, *ω* is the frequency of the harmonic force applied, *φ* is the half-included angle of the indenter tip, *m* is the mass of the indenter, *K*_s is the

spring constant of leaf springs supporting the indenter, and K_f is the stiffness of the indenter. The contact stiffness is then related to the reduced Young's modulus, E_r , by the following relation [13]:

$$E_r = \frac{\sqrt{\pi} S}{2\beta \sqrt{A}}, \quad (2)$$

where β is a constant related to the geometry of the indenter and A is the projected contact area of indentation. The reduced elastic modulus is related to the Young's modulus by [12]:

$$\frac{1}{E_r} = \frac{1 - \nu^2}{E} + \frac{1 - \nu_i^2}{E_i}, \quad (3)$$

where E and ν are the Young's modulus and Poisson's ratio, respectively, and the subscript 'i' refers to the indenter. In this study, E_i was taken as 1,141 GPa and ν_i as 0.07 [14].

FTIR spectrometry

The infrared spectra of the samples were recorded on a Nicolet 4700 Spectrometer (Waltham, MA) in absorption mode. Percentage crystallinity was calculated by measuring the relative absorbance of a crystallinity-band and crystallinity-insensitive band. For PP these bands correspond to absorbance at wavenumbers of 997 and 973 cm^{-1} , respectively [15]. The percentage crystallinity is given by the following formula:

$$\% \text{Crystallinity} = \left(\frac{A_{997}}{A_{973}} \right) \times 100, \quad (4)$$

where A_{997} and A_{973} represent absorbance at wavenumbers of 997 and 973 cm^{-1} , respectively.

Dynamic Young's modulus determination by impulse excitation technique (ASTM E1876-99)

Resonant frequencies for a given specimen are functions of the specimen modulus, mass, and dimensions. This method measures the fundamental resonant frequency of a specimen by exciting it mechanically with an impulse tool. The fundamental resonant frequency, dimensions, and mass of the specimen are then used to calculate dynamic Young's modulus of the specimen by using the following formula [16]:

$$E_f = 0.9465 \times \left(\frac{mf^2}{b} \right) \times \left(\frac{L^3}{t^3} \right) \times T_1, \quad (5)$$

where m is the mass (g), f is the vibration frequency (Hz), L is the length (mm), b is the width (mm), and t ($< b$) is the thickness (mm). T_1 is a correction factor for fundamental flexural mode to account for finite thickness of bar, Poisson's ratio (ν), and is given by the following equation:

$$T_1 = 1 + 6.585 \times (0.0752\nu + 0.8109\nu^2) \times \left(\frac{t}{L} \right)^2 - 0.868 \times \left(\frac{t}{L} \right)^4 - \left(\frac{8.34 \times (1 + 0.2020\nu + 2.173\nu^2) \left(\frac{t}{L} \right)^4}{1 + 6.338 \times (1 + 0.1408\nu + 1.536\nu^2) \left(\frac{t}{L} \right)^2} \right). \quad (6)$$

Results

Visual appearance

The visual appearance of the LFT beams changed as a result of UV exposure. The color of the exposed surface changed from light green to chalky white (see Fig. 2). Surface damage in the form of matrix loss and extensive fiber exposure can be seen.

Optical microscopy

Images of the polished cross section of the UV exposed LFT at different stages of exposure (Figs. 3–5) show the progression of damage. In Fig. 3 cracks appear to start at the surface and propagate inward. Figures 4 and 5, after 400 and 1,600 h of exposure, respectively, show more



Fig. 2 (a) Unexposed beam and (b) UV exposed beam. Damage caused by UV can be seen in the form of many fibers exposed at the surface

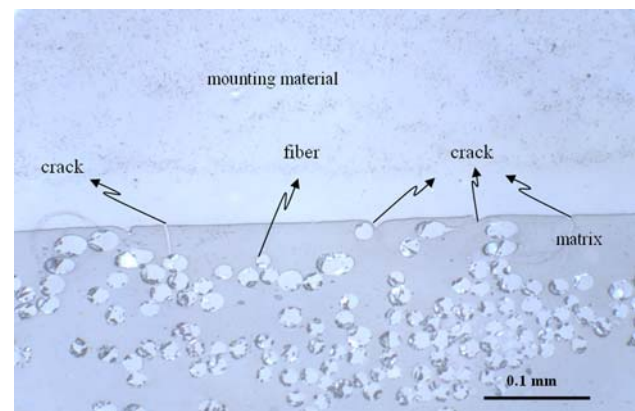


Fig. 3 Polished cross section of the LFT exposed to UV for 100 h. Surface cracks begin to form

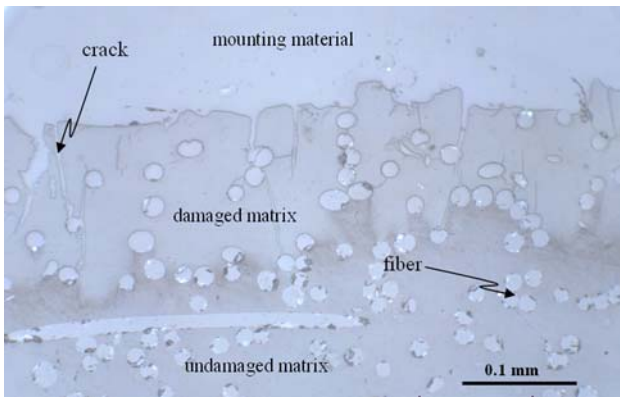


Fig. 4 Polished cross section of the LFT exposed to UV for 400 h. Degraded matrix layer can be easily seen due to easily distinguishable contrast between the degraded layer and the unaffected layer. Surface crack density increases as compared to the density at 100 h

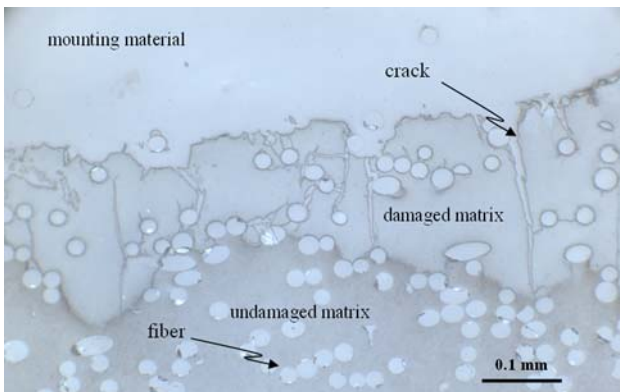


Fig. 5 Polished cross section of the LFT exposed to UV for 1,600 h. Surface crack density is maximum for the sample exposed for 1,600 h

cracks; note also the distinct contrast between the damaged and the undamaged layer. The difference in contrast is indicative of the changes taking place in the matrix due to UV exposure. Similar changes were also found in the case of neat PP (data not shown) with increase in cracks and contrast between the damaged and the undamaged layer.

Scanning electron microscopy

Scanning electron microscopy micrographs showed the degradation of the surface after UV exposure. Microstructure of the unexposed LFT specimen is shown in Fig. 6. The glass fibers are well bonded to the matrix. Damage in the matrix, after 200 h of UV exposure, is evident in Fig. 7 in the form of cracks (long ones along the fiber length and short transverse cracks) can be seen. Some pieces of the matrix as well as debonded fibers can also be observed. The damage after 1,600 h of UV exposure is shown in Fig. 8. Most of the matrix in the surface region

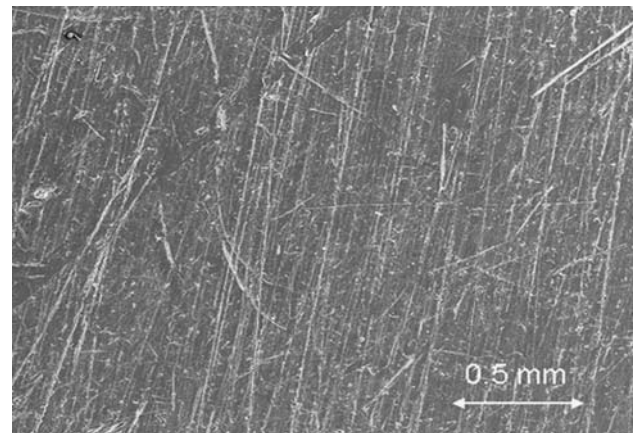


Fig. 6 LFT unexposed to UV radiation. Glass fibers are well bonded with the matrix

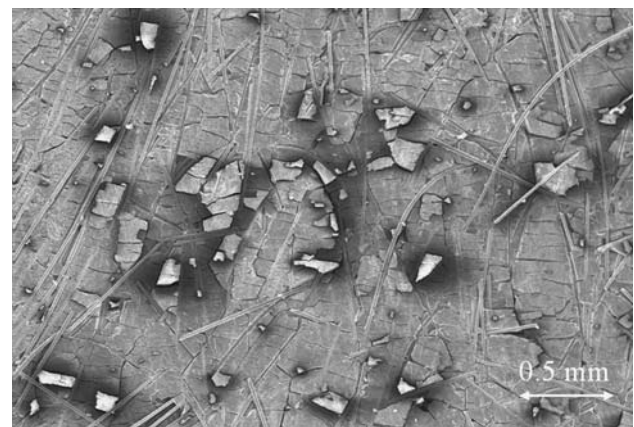


Fig. 7 LFT exposed for 200 h to UV radiation. Matrix damage in the form of cracks can be seen. Fibers start getting exposed to the surface



Fig. 8 LFT exposed for 1,600 h to UV radiation. Most of the matrix in the surface region has disappeared and exposed fibers can be seen

has disappeared and fibers are exposed to the surface. Similar progression of damage with extensive surface cracking was also observed in the case of neat PP.

Nanoindentation

An optical micrograph of the cross section of the LFT exposed to LFT for 1600 h is shown in Fig. 9. The nanoindentation was done in the matrix at different depths from the surface both in the damaged as well as the undamaged region for LFT and neat PP.

Figure 10 shows a representative modulus versus displacement plot for indentation done on the unexposed sample and the sample exposed to UV radiation for 200, 400, and 1,600 h for LFT. It can be seen that the sample exposed to 1,600 h shows higher modulus as compared to the unexposed sample and the samples exposed for 200 and 400 h. These results indicate relative change in the local modulus of PP matrix in the LFT due to UV exposure for different times. Similar plots were also obtained for neat PP (data not shown).

Modulus versus distance from the surface plot for LFT and neat PP can be seen in Figs. 11 and 12, respectively. Each point in the plot is the average of ten indentations, at a given distance from the surface. It can be seen from the plots that at a given distance, the sample exposed to UV for more time has higher modulus values as compared to the samples exposed for lesser time. But, as we go deeper into the sample the modulus for all the samples is about the same. Thus, it is evident that the damage layer formed due to UV degradation is confined, only, to few hundred micrometers from the surface while the material underneath the degraded layer remained unaffected.

Figures 11 and 12 are replotted to show a comparative damage plot between LFT and neat PP for a given exposure time. The results are shown in Figs. 13 and 14 for the

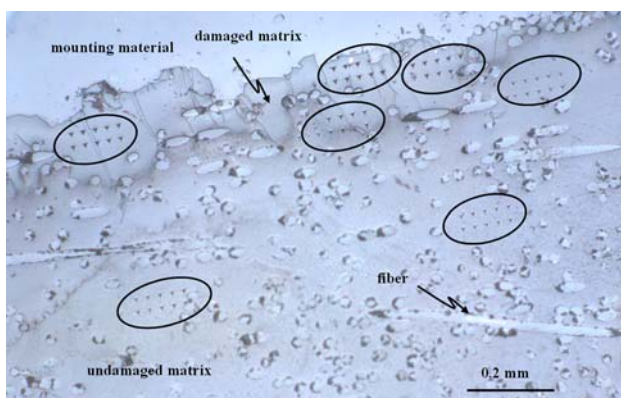


Fig. 9 Polished cross section of the LFT exposed to UV for 1,600 h with nanoindentation marks on it (encircled). Several indentations were done at varying distances from the surface

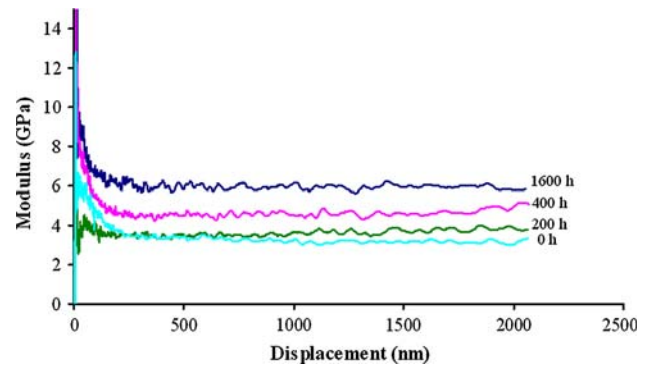


Fig. 10 Representative modulus versus displacement curves for indentation done on the degraded region of the LFT sample exposed to UV radiation for (a) 200 h, (b) 400 h, and (c) 1,600 h. The curve for indentation done on the unexposed sample (0 h) is also shown. The sample exposed to 1,600 h shows the highest modulus

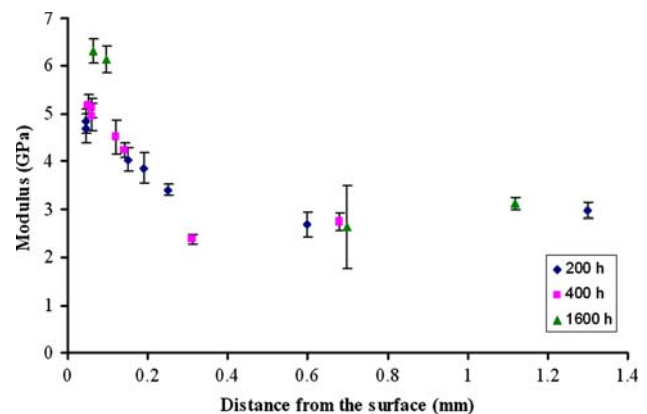


Fig. 11 Modulus versus distance from the surface plots for the samples exposed to UV for (a) 200 h, (b) 400 h, and (c) 1,600 h. Near the surface till about 0.3 mm, the higher the exposure time, the higher the modulus. The modulus value plateaus to 2.5 GPa thereafter

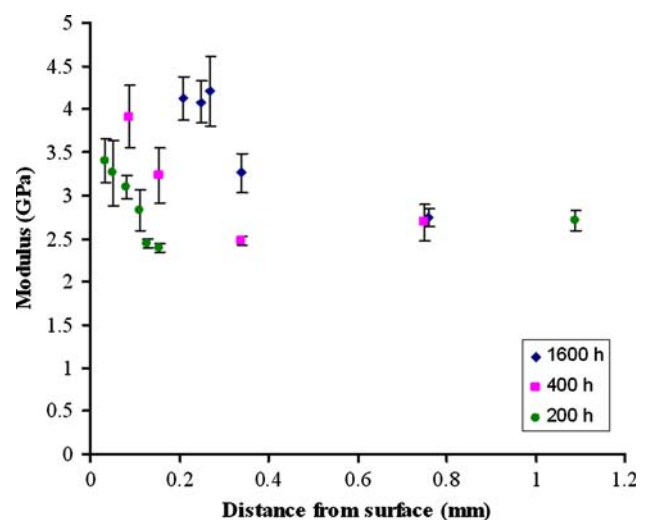


Fig. 12 Modulus versus distance from the surface plots for the PP samples exposed to UV for (a) 200 h, (b) 400 h, and (c) 1,600 h. The plot shows similar behavior as that shown in Fig. 11

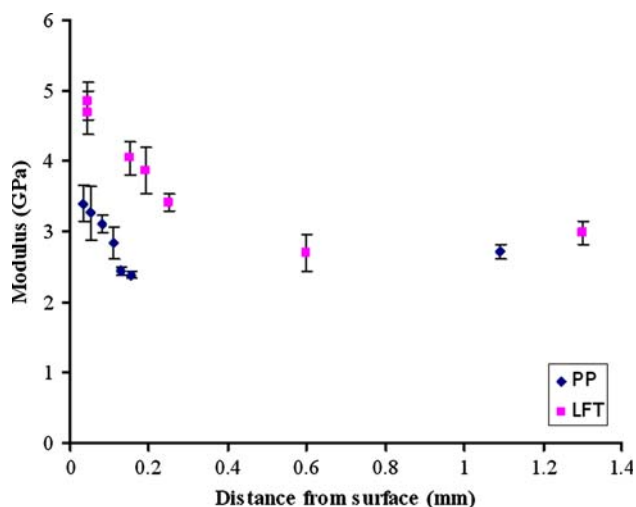


Fig. 13 Modulus versus distance from the surface plots for the PP and LFT samples exposed to UV for 200 h. Till 0.3 mm LFT shows higher change in modulus as compared to that of neat PP. The modulus value plateaus to 2.5 GPa for both after 0.3 mm

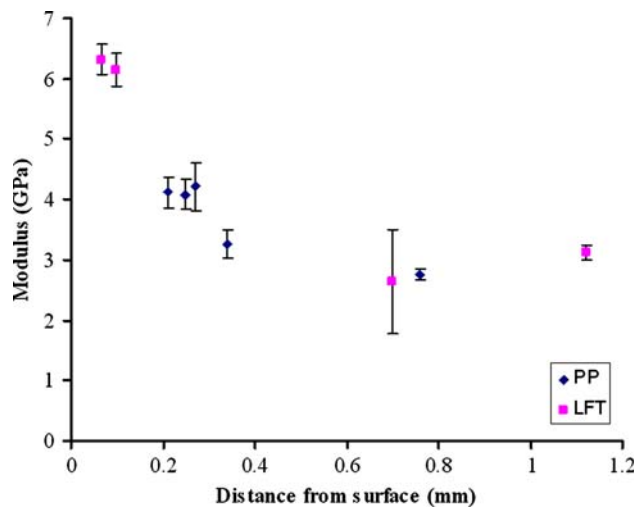


Fig. 14 Modulus versus distance from the surface plots for the PP and LFT samples exposed to UV for 1,600 h. A similar trend as shown in Fig. 12 can be seen

samples exposed to 200 and 1,600 h. It can be clearly seen that for both the plots up to ~0.3 mm, there is more change in the modulus of PP in damaged region of LFT as compared to that in damaged region of neat PP. The modulus value plateaus to 2.5 GPa thereafter, which is the modulus of neat PP, indicating that indents are being made in the undamaged region.

Fourier transform infrared spectrometry

Fourier transform infrared results showed an increase in the intensity of degradation products of PP, i.e., carbonyl and

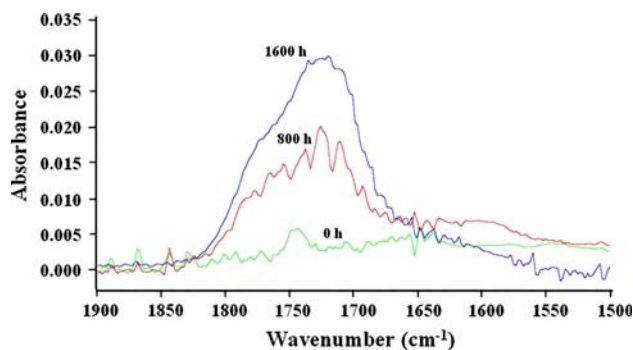


Fig. 15 Absorbance versus wavenumber showing increase in the carbonyl group with UV exposure time

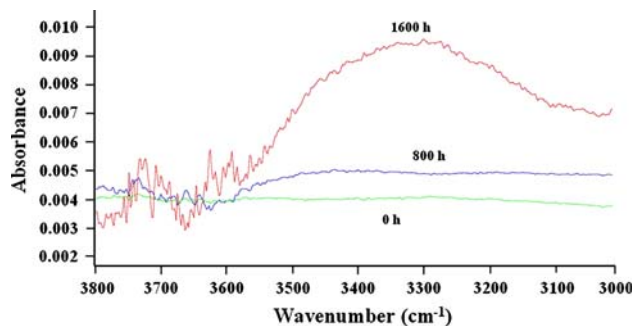


Fig. 16 Absorbance versus wavenumber showing increase in the hydroxyl group with UV exposure time

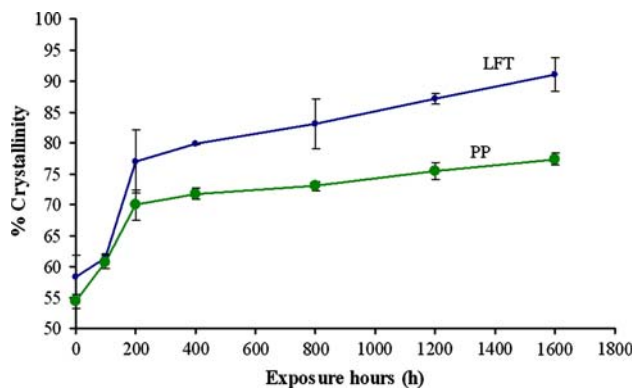


Fig. 17 More change in crystallinity as a function of UV exposure time for LFT as compared to neat PP

hydroxyl bands in the range of 1,900–1,500 and 3,800–3,500 cm^{-1} , respectively (see Figs. 15 and 16). This was as expected since the degradation products increase with increase in exposure time.

From Fig. 17 it can be seen that percentage crystallinity of the unexposed LFT and neat PP increase with the time of UV exposure. The change in crystallinity of PP in the case of LFT is more than that in neat PP. Although, the starting crystallinity is not exactly same since slight variations can

occur in the cooling rate from molten stage, the % change in crystallinity for PP in LFT is 34% to that of 22% in neat PP. This indicates that there is more damage in the surface layer in LFT as compared to that in neat PP.

Damage in LFT

Ultraviolet exposure resulted in cracking of the surface layer (see Figs. 3–8). Amorphous regions have more free volume as compared to crystalline regions. When the broken chains recrystallize, free volume decreases. Following Tong and White [17] we calculate a volume decrease of 4% for the sample exposed for 1,600 h in the current work (see Appendix). Due to this volume decrease, the damaged surface crystalline layer would try to contract but it is inhibited from doing so by the undamaged layer at the bottom [2, 17]. This constraint introduces a tensile stress in the damaged layer and a compressive stress on the undamaged layer (indicated by arrows in Fig. 18). This tensile stress results in transverse cracking in the damaged layer (shown by curve

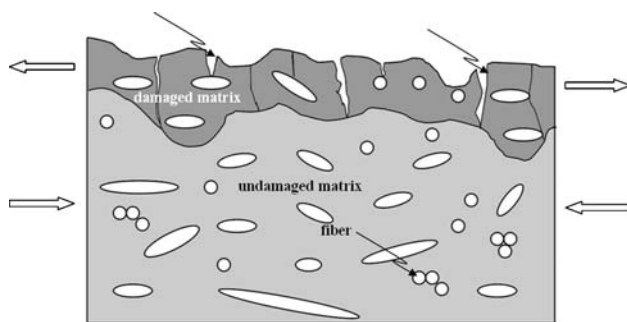


Fig. 18 A schematic showing the UV exposed LFT. The damaged PP matrix at the surface undergoes a reduction in volume compared to the undamaged PP matrix resulting in tensile stress in the damaged layer and a compressive stress in the undamaged PP. The tensile stress results in the formation of transverse cracks in the damaged layer

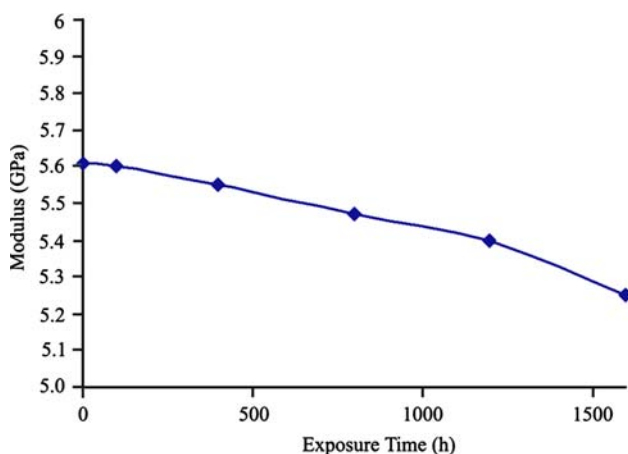


Fig. 19 Modulus versus UV exposure time for the LFT beams. The modulus decreases with exposure time

arrows). Such cracks in a material result in deterioration of the overall mechanical properties. In particular, the presence of cracks or voids results in a loss of elastic modulus. The result of dynamic Young's modulus measurements by impulse excitation as a function of UV exposure is shown in Fig. 19. It can be seen that modulus decreases continuously with increasing UV exposure.

Further discussion

Fourier transform infrared results showed an increase in the intensity of hydroxyl and carbonyl bands with UV exposure time (see Fig. 15 and 16) in LFT indicating different photo-oxidation products of PP in the LFT. The crystallinity of the PP in the damaged region showed an increase with exposure time (see Fig. 17) for both neat PP and LFT. But, PP degrades faster when glass fibers are present, i.e., in the case of LFT than in the case of neat PP. This increase in crystallinity can be explained by chemocrystallization for both the cases, wherein UV degradation causes scission of amorphous molecular chains followed by an increase in crystallinity because of the ease of rearrangement of smaller chains. The effect of glass fibers can be explained as follows. When we add glass fibers to PP, i.e., in the case of LFT, we are adding more chromophores in the PP in the form of functional groups present in the sizing applied to the glass fibers for better bonding with PP. These chromophores accelerate the photo-oxidation of PP and hence we see more damage in the surface layer of LFT in terms of greater change in crystallinity and modulus. Similar results were observed by Selden et al. [5] in the case of wood fibers reinforced PP which underwent more degradation due to the addition of naturally present chromophores in wood fibers in neat PP.

The UV-degraded regions of the LFT samples exposed for larger time showed higher local modulus than the ones exposed for lesser times (see Fig. 10). From Fig. 11 we see that the samples exposed for 1,600 h showed the highest local modulus as a function of the distance from the surface. As the distance from the surface increased the modulus value attained a plateau of 2.5 GPa. These results show that the damage due to UV was confined only to a surface region of thickness 300 μm . Similar trend was observed in the case of neat PP (see Fig. 12). When these results are replotted to compare the local modulus change of PP matrix in LFT and neat PP we see that PP in LFT showed more damage than neat PP (Figs. 13 and 14). Initially for the first 300 μm the PP matrix in LFT underwent more modulus change as compared to neat PP for both the samples (200 and 1,600 h) but later the modulus values of both neat PP and PP matrix in LFT leveled to 2.5 GPa which was expected since the indents were then being made in the undamaged matrix. Thus, results of

nanoindentation corroborate the FTIR results indicating that increase in modulus of the degraded layer can be attributed to the increase in crystallinity of the degraded layer.

It is important to realize that one of the consequences of the chemi-crystallization is the formation of surface cracks [8–11]. Optical micrographs (Figs. 3–5) show the evolution of surface cracks as a function of UV exposure time, along with the development of a distinct contrast between the exposed and the unaffected layer, indicating the microstructural changes taking place in the PP matrix in the LFT. SEM micrographs (see Figs. 6–8) also show the changes taking place on the surface of LFT due to UV exposure. Surface cracks along with the fibers exposed on the surface were observed.

Although, the local modulus of the degraded layer increased with the exposure time, the modulus of the overall composite (LFT) showed a decrease (see Fig. 16). This is because of the formation of surface cracks. Due to chemicrystallization, % crystallinity of the sample increased. This increase in crystallinity in the damaged surface layer led to a contraction in volume by 4 and 2.7% for LFT and neat PP, respectively (see Appendix), compared to the undamaged PP. This volume change resulted in the formation of cracks which decreased the modulus of the overall composite.

Conclusions

The following conclusions can be drawn from this work.

- FTIR results showed an increase in degree of crystallinity of 34% for LFT and 22% for neat PP.
- Nanoindentation results showed that modulus of the degraded region increased with the increase in the exposure time. PP present in LFT underwent more modulus change near the surface region as compared to neat PP. This is probably because of the acceleration of the damage caused by the addition of more chromophores in terms of functional groups present in the sizing applied to the glass fibers for better bonding with neat PP.
- The damaged PP matrix at the surface underwent a reduction in volume compared to the undamaged PP matrix resulting in tensile stress in the damaged layer and a compressive stress in the undamaged PP. The tensile stress resulted in the formation of transverse cracks in the damaged layer. This surface cracking resulted in the observed decrease of dynamic Young’s modulus of the overall LFT.

Acknowledgements Financial support for this work was received from Federal Transit Administration (FTA), contract #AL-26-7022-02. Thanks are due to S.D. Bartus and S. Pillay for providing the LFT plates. Thanks are also due to K. Carlisle for helpful discussions.

Appendix 1

Change in volume of PP due to chemicrystallization

The total volume of PP is sum of amorphous and crystalline parts. Prior to UV exposure, the volume V_o of PP is given by:

$$V_o = \frac{m_{co}}{\rho_c} + \frac{m_{ao}}{\rho_a} \tag{7}$$

where m_{co} and m_{ao} are the masses of the crystalline and amorphous fractions, respectively, and ρ_c and ρ_a are the densities of the crystalline and amorphous phases, respectively.

The initial crystalline mass fraction is given by:

$$f_c = \frac{m_{co}}{m_{co} + m_{ao}} \tag{8}$$

The volume after UV exposure is given by:

$$V_{UV} = \frac{m_c}{\rho_c} + \frac{m_a}{\rho_a}, \tag{9}$$

where m_c and m_a are the masses of the crystalline and amorphous fractions after UV exposure, respectively.

After UV exposure the crystalline mass fraction of PP increases by Δf_c , therefore, we can write:

$$f_c + \Delta f_c = \frac{m_c}{m_c + m_a} \tag{10}$$

From Eqs. 8 and 10, we obtain

$$\Delta f_c = \frac{m_c - m_{c,o}}{m_c + m_a} \tag{11}$$

From Eqs. 7, 9, and 11, we can write for the volume change as:

$$V_o - V_{UV} = \Delta V = \Delta f_c (m_c + m_a) \left(\frac{1}{\rho_c} - \frac{1}{\rho_a} \right) \tag{12}$$

For the sample exposed for 1,600 h, $\Delta f_c = 0.34$ and 0.22 for LFT and neat PP, respectively (from FTIR result, see “FTIR spectrometry” section). For the same sample, we have $m_c + m_a = 21$ g, $\rho_c = 0.936$ g/cm³ and $\rho_a = 0.850$ g/cm³ [18].

From the dimensions of the LFT beam, we have:

$$V_o = 17.59 \text{ cm}^3.$$

Therefore, substituting these values in Eq. 12 we get:

% volume change = 4% for LFT and 2.7% for neat PP.

References

1. Bartus SD, Vaidya UK (2005) Compos Struct 67:263
2. Chawla KK (1998) Composite materials: science and engineering, 2nd edn. Springer-Verlag, New York

3. Qureshi FS, Amin MB, Maadhah AG, Hamid SH (1990) *J Polym Eng* 9:67
4. Yakimets I, Lai D, Guigon M (2004) *Polym Degrad Stab* 86:59
5. Selden R, Nystrom B, Langstrom R (2004) *Polym Compos* 25:543
6. Lundlin T, Cramer SM, Falk RH, Felton C (2004) *J Mater Civil Eng* 16:547
7. Lundlin T, Falk RH, Felton C (2001) Proceedings of the 6th International Woodfiber-Plastic Composites Conference, Forest Products Society, May, Madison, Wisconsin, p 87
8. Rabello MS, White JR (1997) *Polym Degrad Stab* 56:55
9. Larena A, Jiménez De Ochoa S, Domínguez F (2006) *Polym Degrad Stab* 91:940
10. Rabello MS, White JR (1997) *Polymer* 38:6379
11. White JR, Turnbull A (1994) *J Mater Sci* 29:584
12. Oliver WC, Pharr GM (1992) *J Mater Res* 7:1564
13. Li X, Bhushan B (2002) *Mater Charact* 48:11
14. Simmons G, Wang H (1971) *Single crystal elastic constants and calculated aggregate properties: a handbook*. MIT Press, Cambridge, MA
15. Karger-Kocsis J (ed) (1999) *Polypropylene: an A-Z reference*. Kluwer Academic Publishers, The Netherlands
16. ASTM E 1876-99 (1999) *Annual book of ASTM standards*. American Society for Testing and Materials
17. Tong L, White JR (1997) *Polym Eng Sci* 37:321
18. Signor AW, Vanlandingham MR, Chin JW (2003) *Polym Degrad Stab* 79:359